Raman Observation of the Interactions between NH_4^+, SO_4^{2-}, and H_2O in Supersaturated $(NH_4)_2SO_4$ Droplets

Jin-Ling Dong, Xiao-Hong Li, Li-Jun Zhao, Han-Shuang Xiao, Feng Wang, Xin Guo, and Yun-Hong Zhang*

The Institute for Chemical Physics, Beijing Institute of Technology, Beijing, China 100081

Received: April 10, 2007; In Final Form: July 6, 2007

High signal-to-noise ratio (S/N) Raman spectra of $(NH_4)_2SO_4$ droplets deposited on a quartz substrate were obtained from dilute to supersaturated states upon decreasing the relative humidity (RH). When the molar water-to-solute ratio (WSR) decreases from 16.8 to 3.2, the υ_1-SO_4^{2-} band changes very little, that is, showing a red-shift of only about 1 cm^{-1} (from 979.9 to 978.8 cm^{-1}) and an increase of its full width at half-maximum (fwhm) from 8.3 to 9.8 cm^{-1}. Other vibration modes such as υ_2- and υ_4-SO_4^{2-} bands appear almost constantly at 452 and 615 cm^{-1}. Such kind of a spectroscopic characteristic is different from previous observation on other cations, indicating that the interactions between SO_4^{2-} and NH_4^+ in supersaturated states are similar to those between SO_4^{2-} and H_2O in dilute states. After fitting the Raman spectra with Gaussian functions in the spectral range of 2400−4000 cm^{-1}, we successfully extracted six components at positions of 2878.7, 3032.1, 3115.0, 3248.9, 3468.4, and 3628.8 cm^{-1}, respectively. The first three components are assigned to the second overtone of NH_4^+ umbrella bending, the combination band of NH_4^+ umbrella bending and rocking vibrations, and the NH_4^+ symmetric stretching vibration, while the latter three components are from the strongly, weakly, and slightly hydrogen-bonded components of water molecules, respectively. With a decrease of the RH, the proportion of the strongly hydrogen-bonded components increases, while that of the weakly hydrogen-bonded components decreases in the droplets. The coexistence of strongly, weakly, and slightly hydrogen-bonded water molecules must hint at a similar hydrogen-bonding network of NH_4^+, SO_4^{2-}, and H_2O to that of pure liquid water in supersaturated $(NH_4)_2SO_4$ droplets.

Introduction

$(NH_4)_2SO_4$ has long been known to be one of the major components of atmospheric aerosols.[1−3] On the basis of measurements at several sites, Heintzenberg has suggested an average amount of ammonium and sulfate of 8% and 28% by weight in urban fine particles, respectively.[4] According to some estimations, the particles composed of SO_4^{2-}, NO_3^-, NH_4^+, and H^+ are the most significant anthropogenic contribution to the global accumulation mode aerosol.[5] Moreover, theoretical studies show that $(NH_4)_2SO_4$ aerosols have an important effect on the formation of cirrus cloud which cover about 30% of Earth and may warm or cool Earth, depending on the altitude and its optical density.[6,7] In addition, $(NH_4)_2SO_4$ aerosols can effectively affect atmospheric chemistry by providing sites for heterogeneous reactions such as N_2O_5 hydrolysis.[8] Furthermore, Hu and Abbatt found the reactivity of the hydrolysis reaction is relatively high at relative humidities (RHs) well below the deliquescence point of $(NH_4)_2SO_4$, that is, in the supersaturated states.[9]

Due to its ubiquitous presence and significant role, $(NH_4)_2SO_4$ in aerosol form has been widely studied, especially its water uptake and evaporation behaviors as a function of RH at ambient temperatures. Various techniques have been employed, such as particle mobility,[10] optical particle scattering technique,[11] electrodynamic balance (EDB),[12] and infrared spectroscopy.[13] By using the single-particle levitation technique, Tang et al. determined that the deliquescence and crystallization RHs are 80 and 37%, respectively, in the growth and evaporation cycle of the single $(NH_4)_2SO_4$ aerosol particle at 25 °C,[14] in good agreement with several other observations.[15−18] Parsons et al. used a flow cell coupled with an optical microscope to study the deliquescence and crystallization of $(NH_4)_2SO_4$ particles internally mixed with water-soluble organic compounds.[19] Combining aerosol flow tube (AFT) with infrared spectroscopy, submicrometer aqueous $(NH_4)_2SO_4$ particles containing hematite and corundum inclusions were investigated and a strong dependence of the crystallization RH on the inclusion size was disclosed.[20]

Even though the formation of contact ion pairs (CIPs) in several aqueous solutions of $Al_2(SO_4)_3$, $CdSO_4$, and $FeSO_4$ has been investigated with spectroscopy by selecting the bulk $(NH_4)_2SO_4$ solutions as a model of undisturbed sulfate ions,[21−23] detailed interactions of NH_4^+−SO_4^{2-}, NH_4^+−H_2O, and SO_4^{2-}−H_2O are not clear in supersaturated states, which basically determine the hygroscopic properties and thus the reactivity of the supersaturated $(NH_4)_2SO_4$ aerosols as a micro-reaction-container for N_2O_5 hydrolysis.[8,9] Zhang and Chan have obtained Raman spectra of levitated $(NH_4)_2SO_4$ droplets in an EDB cell;[24] however, the spherical levitated $(NH_4)_2SO_4$ droplets showed strong physical morphology-dependent resonances (MDRs) confusing the fine spectral changes induced by chemical interactions between NH_4^+ and SO_4^{2-}.

In this paper, we report on the confocal Raman spectra of individual $(NH_4)_2SO_4$ droplets deposited on a quartz substrate. By decreasing the ambient RH, supersaturated states can be easily achieved for the $(NH_4)_2SO_4$ droplets. At the same time,

* Author to whom correspondence should be addressed. Tel.: 86-10-86668406. Fax: 86-10-68912652. E-mail: yhz@bit.edu.cn.

10.1021/jp072772o CCC: $37.00
Published on Web 10/05/2007

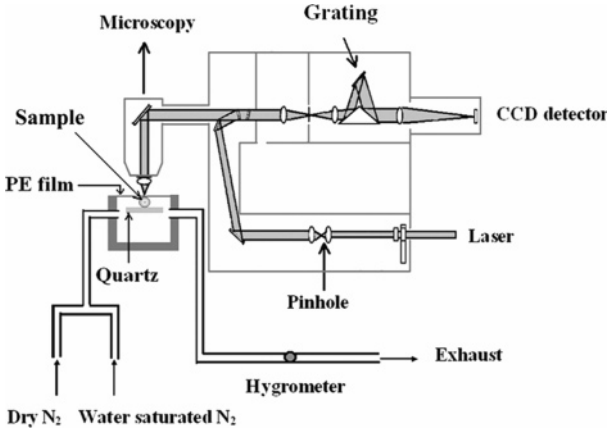

Figure 1. Experimental setup for the micro-Raman measurements of $(NH_4)_2SO_4$ droplets deposited on quartz substrate.

no physical MDR disturbance is apparent in the spectra of the deposited $(NH_4)_2SO_4$ droplets with a half-ellipsoidal shape rather than a regular sphere. Thus, the Raman spectra with high signal-to-noise (S/N) ratios can be obtained. Referring to the evolutions of the υ_1-SO_4^{2-} band, insightful discussions will be made on the interactions between NH_4^+ and SO_4^{2-} in supersaturated states. In order to investigate the water structures in the $(NH_4)_2SO_4$ droplets, we attempt to separate the vibrational bands of NH_4^+ from the O−H stretching bands in the region of 2400−4000 cm^{-1} by fitting the Raman spectra of $(NH_4)_2SO_4$ droplets. The ultimate aim of this study is to understand the interactions between ions and those between ions and water molecules in $(NH_4)_2SO_4$ droplets, especially in supersaturated states on a molecular level.

Experimental Section

Raman Spectra Measurement of $(NH_4)_2SO_4$ Droplets. The technique used in this work has been described elsewhere.[25] A schematic diagram of the experimental apparatus is shown in Figure 1. It consists mainly of two functioning parts, that is, a chamber for adjusting the ambient RH of $(NH_4)_2SO_4$ droplets and a micro-Raman system (Ranishaw Invia) for measuring Raman spectra and imaging morphological changes of the droplets.

A stock solution of 1.0 mol/L $(NH_4)_2SO_4$ was prepared by dissolving analytical-grade crystalline $(NH_4)_2SO_4$ in deionized water without further purification. By using a syringe, droplets of the solution were injected and sprayed onto a quartz substrate fixed to the bottom of the chamber. Then, the chamber was sealed with a piece of transparent polyethylene (PE) film. The RH in the chamber could be precisely controlled by mixing and adjusting two flows of dry and water-saturated nitrogen gas. The real-time RH could be monitored by the humidity temperature meter (Centertek Center310) with an accuracy of ±2.5% RH and ±0.7 °C.

After being stabilized for about 1 h at given RHs of the chamber, the micro-Raman measurement was made for droplets in diameters from ~30 to ~100 μm, as observed through a 50× objective of the Leica DMLM microscope. The 514.5 nm line of an argon-ion laser with an output power of 20 mw was used as an excitation source. Before the Raman measurement of the droplets, a calibration was made with respect to the 520 cm^{-1} silicon band. A 514.5 nm Raman notch filter was used to remove the strong Rayleigh scattering. The backscattering signals passing through a 1800 g/mm grating of the monochromator were subsequently detected and recorded by a charge-coupled device (CCD). The Raman spectra with 1 cm^{-1} resolution from

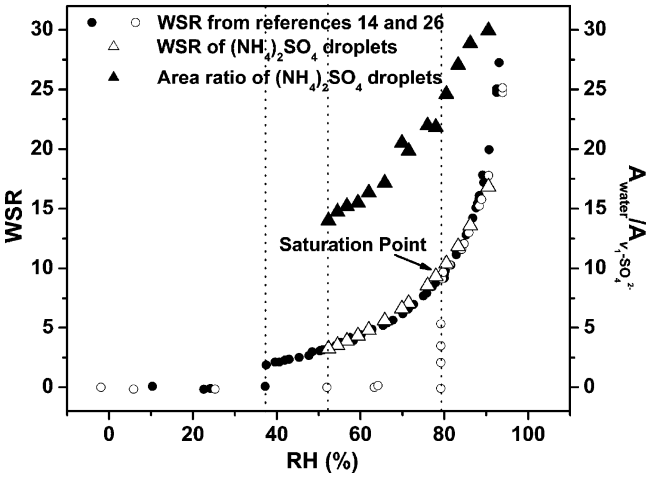

Figure 2. Water activity data of $(NH_4)_2SO_4$. Solid triangle: area ratio of water envelope to the υ_1-SO_4^{2-} band in the dehumidifying process; open triangle: WSR obtained in this work by referring RH to previous results of WSR vs RH in refs 14 and 26; solid and open cycles: WSR of the $(NH_4)_2SO_4$ droplet in dehumidifying and humidifying processes from refs 14 and 26.

100 to 4000 cm^{-1} were obtained with the grating operating 5 scans, and each with an accumulation time of 10 s. All measurements were made at ambient temperatures of 22−24 °C. The morphological changes of the selected droplets were monitored by the Leica DMLM microscope.

Spectra Fitting. In order to obtain the information on the interactions between NH_4^+, SO_4^{2-}, and H_2O in supersaturated $(NH_4)_2SO_4$ droplets, the evolution of the vibrational bands of NH_4^+ ions and the O−H stretching envelope of water must be separated from each other. In practice, nonlinear curve fittings were performed by Origin 7.0 software in the range of 2400−4000 cm^{-1} for all the obtained spectra with the Gaussian function as follows being selected for nonlinear curve-fitting functions.

$$y = y_0 + \frac{A}{w\sqrt{\pi/2}} e^{-2(x-x_0)^2/w^2}$$

where, y_0 is the baseline offset, A is the total area under the curve from the baseline, x_0 is the center of the peak, w is 2 "sigma", approximately 0.849 the full width of the peak at half-maximum (fwhm). This function describes a bell-shaped curve like the normal (Gaussian) probability distribution. The center x_0 represents the "mean", while $w/2$ is the standard deviation. The aim of fitting is to find out those values of the parameters which best describe the experimental Raman spectra.

Results and Discussion

Supersaturated $(NH_4)_2SO_4$ Droplets on the Quartz. The molar water-to-solute ratios (WSRs) of $(NH_4)_2SO_4$ particles at various RHs are displayed in Figure 2, including those for a saturation point of 80% RH and an efflorescence point of 37% RH.[14,26] The WSRs of this work at given RHs can be evaluated by referring to refs 14 and 26 and are shown as open triangles in Figure 2. It can be seen that the deposited $(NH_4)_2SO_4$ droplets can break through the saturation point (WSR = 9.6 at 80% RH) and enter into the supersaturated region, similar to the levitated ones.[14,26] When the RH reaches a fairly low value (52%), the droplet with WSR = 3.2 still does not effloresce on the quartz, indicating a $H_2O/NH_4^+/SO_4^{2-}$ ratio of about 3:2:1 in this supersaturated droplet. This supersaturated state with such a low

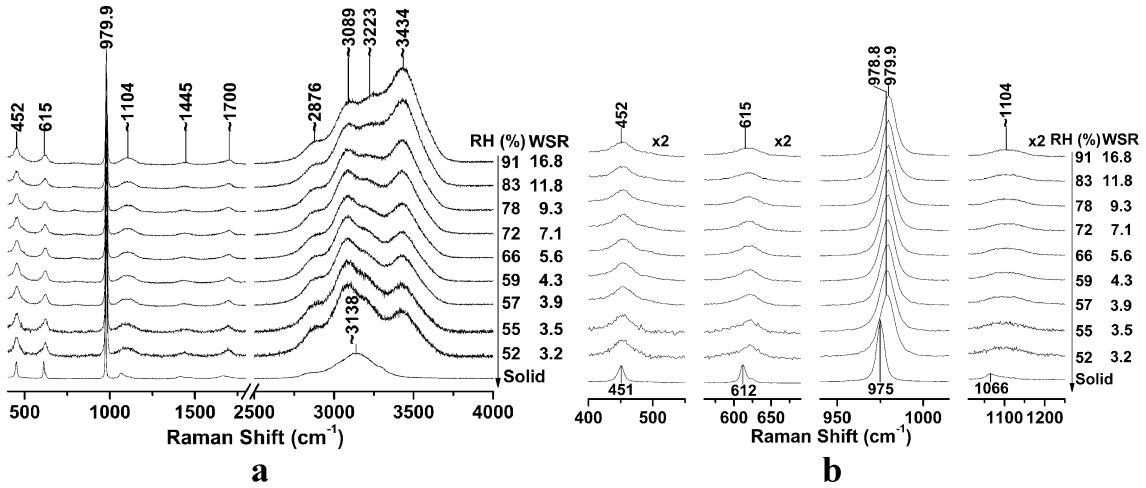

Figure 3. (a) Raman spectra of $(NH_4)_2SO_4$ droplets, and (b) the enlarged Raman bands of SO_4^{2-} in $(NH_4)_2SO_4$ droplets at various RH values.

WSR facilitates effectively the formation of CIPs between SO_4^{2-} and NH_4^+, which can be detected by confocal Raman spectroscopy.

Raman Spectra of the $(NH_4)_2SO_4$ Droplets. Free SO_4^{2-} (aq) has T_d symmetry and nine modes of internal vibration spanning the representation: $\Gamma_{vib}(T_d) = A_1 + E + 2F_2$. All vibrational modes are Raman-active, but only F_2 modes are IR-active. The spectra of $(NH_4)_2SO_4$ aerosols at various RHs in the dehumidifying process are included in Figure 3a. The enlarged vibrational bands of SO_4^{2-} are shown in Figure 3b. All the spectra are normalized to the intensity of the υ_1-SO_4^{2-} band. Four predicted bands of SO_4^{2-}, identified as the totally symmetric mode υ_1 (A_1) at 979.9 cm^{-1}, the antisymmetric stretching mode υ_3 (F_2) at ~1104 cm^{-1}, the bending modes υ_2 (E) at 452 cm^{-1}, and υ_4 (F_2) at 615 cm^{-1}, respectively, are clearly observed in the spectrum of the dilute droplets at 91% RH in Figure 3. For comparison, the spectrum of crystallized $(NH_4)_2SO_4$ particles in this work is also displayed and marked with "Solid" in Figure 3, in which the υ_1-, υ_2-, υ_3-, and υ_4-SO_4^{2-} bands appear at 975, 451, 612, and 1066 cm^{-1}, respectively. The complicated envelope in the spectral region of 2400−4000 cm^{-1} results from the total contributions of H_2O and NH_4^+ vibrational modes.

The υ_1-SO_4^{2-} band has been generally observed to be sensitive to cation types, salt concentrations, and temperatures.[22,23,27−29] However, in this work as seen in Figure 3b, the υ_1-SO_4^{2-} band changes only slightly with decreasing the RH. Figure 4 shows the peak position and the fwhm of the υ_1-SO_4^{2-} band for $(NH_4)_2SO_4$ droplets as a function of WSR. The υ_1-SO_4^{2-} band of $(NH_4)_2SO_4$ droplets has a red-shift in peak position from 979.9 to 978.8 cm^{-1} and an increase in its fwhm from 8.3 to 9.8 cm^{-1} when the WSR decreases from 16.8 to 3.2 (from 91 to 52% RH). The peak position of this band shifts to 975 cm^{-1} with an abrupt increase in its intensity when an anhydrous crystal begins to form. The trend of downward shift of the υ_1-SO_4^{2-} band in $(NH_4)_2SO_4$ droplets with decreasing RH is in good agreement with the result reported by previous work,[24] which showed a red-shift from 981 to 977 cm^{-1} for the υ_1-SO_4^{2-} band in the levitated $(NH_4)_2SO_4$ droplets when the WSR decreased from 15.8 to 1.7. The larger red-shift of the υ_1-SO_4^{2-} band in previous work is probably due to the more supersaturated states achieved in the levitated droplets (with the lowest WSR of 1.7) than in the deposited ones (with the lowest WSR of 3.2), because the levitated droplets in the center of an EDB can eliminate the heterogeneous nucleation to a great extent. Contrary to the linear dependence of the peak position on salt concentration ($\upsilon_{max} = 980.89 + 0.176C_{SO_4^{2-}}$) in dilute bulk $(NH_4)_2SO_4$ solutions,[22] the peak position is found to red-shift with increasing the concentration in supersaturated $(NH_4)_2SO_4$ droplets.

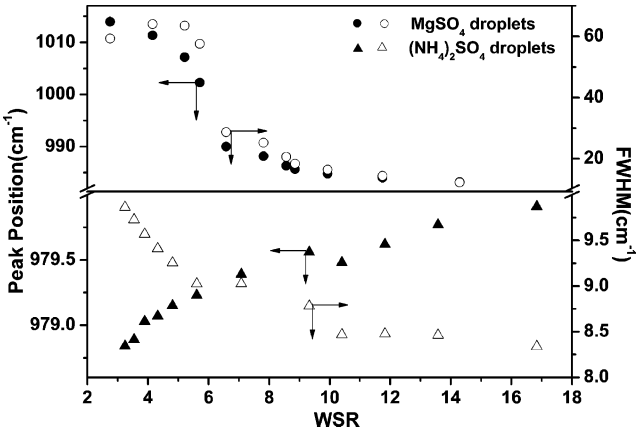

Figure 4. Peak position and fwhm of the υ_1-SO_4^{2-} band of $(NH_4)_2SO_4$ and $MgSO_4$ droplets as a function of WSR. Circle: $MgSO_4$ droplets. Triangle: $(NH_4)_2SO_4$ droplets. Solid symbols: the peak positions of the υ_1-SO_4^{2-} band. Open symbols: the FWHMs of the υ_1-SO_4^{2-} band.

In order to understand the interactions between NH_4^+ and SO_4^{2-}, especially in supersaturated states, we also show the detailed changes of the υ_1-SO_4^{2-} band of $MgSO_4$ droplets deposited on quartz for comparison in Figure 4. The peak position of the υ_1-SO_4^{2-} band of dilute $MgSO_4$ droplets centers around 983 cm^{-1}. As the RH decreases from 96 to 4%, the υ_1-SO_4^{2-} band of $MgSO_4$ shows a blue-shift of 38 cm^{-1} from 983 to 1021 cm^{-1}, and an increase in its fwhm of 43.9 cm^{-1} from 10.3 to 54.2 cm^{-1}, both of which are about 30 times the values of those for $(NH_4)_2SO_4$ droplets. Mg^{2+} has a large charge-to-radius ratio and can form various CIPs with SO_4^{2-} in concentrated $MgSO_4$ droplets, that is, monodentate CIPs, bidentate CIPs, and more complex structures such as chain structures.[25] When polyatomic anions such as SO_4^{2-} enter the first hydration sphere of cations, marked changes will occur in the spectrum of ligated sulfate, according to which ligated and unligated sulfate can be identified.[30] With the formation of various CIPs, the symmetry of SO_4^{2-} decreases and three new bands emerge accordingly, resulting in a blue-shift of peak position and an increase of fwhm of υ_1-SO_4^{2-}. For dilute sulfate solutions, the correlation between the peak position, cation species, and concentration is the result of the changes in the local potential field experienced by SO_4^{2-} in the presence of

TABLE 1: Vibrational Spectra of NH_4^+ and H_2O in the Range of 2700−3800 cm^{-1} in Previous Literature

	solution[a,b]	solid[c]	assignment
NH_4^+	2878.7	3041.0	second overtone of NH_4^+ umbrella bending
	3032.1		combination band of NH_4^+ umbrella bending and rocking
	3115.0		NH_4^+ symmetric stretch
	3215.0	3138.0	NH_4^+ asymmetric stretch
H_2O	3248.9		strongly hydrogen-bonded components
	3468.4		weakly hydrogen-bonded components
	3628.8		slightly hydrogen-bonded components

[a] Ref 35. [b] Ref 36. [c] Ref 34.

the cation field.[22] At the same time, the charge-to-radius ratio determines the extent of change in the local potential field. Therefore, the frequency difference of the υ_1-SO_4^{2-} band between dilute $(NH_4)_2SO_4$ (979.9 cm^{-1}) and $MgSO_4$ (983 cm^{-1}) solutions can be attributed to the differences in the ionic charges and radii of NH_4^+ and Mg^{2+} as well as to their effects on hydrated water.

With an increase of the concentration, the peak position of the υ_1-SO_4^{2-} band red-shifts only slightly for $(NH_4)_2SO_4$, while it blue-shifts noticeably for $MgSO_4$. Watanabe and Hamaguchi attributed the distinction to the classification of ions by Frank and Wen,[31] who regarded Mg^{2+} and NH_4^+ as "structure maker" and "structure breaker", respectively, by considering the effect of surrounding water molecules on ion association. Vollmar explained the relatively unchanged υ_1-NO_3^- band of NH_4NO_3 from the viewpoint of hydrogen bonds.[32] Several studies found that the formation of a hydrogen bond resulted in a red-shift of the frequency of the symmetric vibration of the base (here, υ_1-SO_4^{2-}) in the hydration process. Vollmar believed it reasonable if the attached molecule simply increased the effective mass of the vibrating units (the O atoms in both NO_3^- and SO_4^{2-}).[32] Although the frequency change may be caused wholly or partly by a weakening of the force constant of the bond, he concluded that replacement of H_2O molecules hydrogen-bonded with O of NO_3^- by NH_4^+ ions would leave the frequency of υ_1-NO_3^- relatively unchanged.[32] Considering the positive charge possessed by NH_4^+, we suggest that the hydrogen bonds between SO_4^{2-} and NH_4^+ are a little stronger than those between SO_4^{2-} and H_2O. Therefore, the effective mass of the O atom in SO_4^{2-} will be slightly larger when the H_2O molecules hydrated with SO_4^{2-} are replaced by NH_4^+, which leads to a small red-shift of the bond frequency.

Compared with Mg^{2+}, NH_4^+ ion has a lower charge-to-radius ratio and accordingly a less electrostrictive effect on water. Therefore, $(NH_4)_2SO_4$ solutions have been considered to be a model of undisturbed SO_4^{2-} in which the υ_1-SO_4^{2-} band is not sensitive to concentration variations. When the WSRs are smaller than the number of water molecules required to fill in the first hydration shell of NH_4^+, CIPs between NH_4^+ and SO_4^{2-} are expected to occur in abundance. For example, Zhang and Chan have suggested the existence of CIPs in $(NH_4)_2SO_4$ droplets with WSRs between 3.9 and 1.5.[24] According to either theoretical considerations or experimental results, the accessible WSR of 3.2 is low enough to facilitate the formation of CIPs in this work. Since there is only a small peak position shift (1.1 cm^{-1}) and limited broadening (1.5 cm^{-1}) of the υ_1-SO_4^{2-} band, it can be concluded that the formation of CIPs between NH_4^+ and SO_4^{2-} has little effect on the υ_1-SO_4^{2-} band. In other words, there is little difference between NH_4^+ and H_2O interacting with SO_4^{2-}. It proves that $(NH_4)_2SO_4$ solutions are valid as the model of undisturbed SO_4^{2-} not only in dilute but also in supersaturated states. It seems counterintuitive that little difference was observed in the υ_1-SO_4^{2-} band although Coulombic interactions should exist between SO_4^{2-} and NH_4^+ when CIPs were formed. The reason may be that the Coulomb force is fairly small because of the large volumes and symmetrical distribution of the charges for the tetrahedral NH_4^+. In addition, the hydrogen bonds formed by NH_4^+ and SO_4^{2-} may help to partly offset the electrostatic interactions by maintaining the tetrahedral geometry of SO_4^{2-}, because the tetrahedral NH_4^+ was found to fit quite well into the network of water.[33] A contrasting cation is Mg^{2+}, whose interactions with SO_4^{2-} have been found to drastically affect the vibrational modes of SO_4^{2-} in solutions,[25] probably because of the relatively large charge-to-radius ratio of Mg^{2+}, as well as the lack of hydrogen bonds with SO_4^{2-}.

On the basis of the fact that the υ_3-SO_4^{2-} band is highly sensitive to the various environments in solutions, for example, those caused by the different hydrated structures of SO_4^{2-},[25] the broadening (from 82.0 cm^{-1} at WSR = 16.8 to 103.8 cm^{-1} at WSR = 3.2) of the υ_3-SO_4^{2-} band in our work, especially at the low RHs, should be attributed to the complexity of the environment of SO_4^{2-}. An interesting fact is that the response of the two bending modes of υ_2- and υ_4-SO_4^{2-} is also not sensitive to the formation of CIPs.

Separation of H_2O Stretching Bands from NH_4^+ Vibrations. Just like SO_4^{2-}, the free NH_4^+ ion has T_d symmetry and nine internal vibrational modes, spanning the representation of $\Gamma_{vib} = A_1 + E + 2F_2$. The symmetric stretching vibration (υ_1), asymmetric one (υ_3), and the two bending vibrational modes (υ_2 and υ_4) of NH_4^+ appear at 3061, 3131, 1661, and 1416 cm^{-1}, respectively, as observed by Jordanov and Zellner by means of optical levitation and Raman spectroscopy.[34] For the Raman spectra of $(NH_4)_2SO_4$ droplets in the 2400−4000 cm^{-1} region, there is a complicated envelope contributed by both NH_4^+ and H_2O, as shown in Figure 3a. In order to extract the bands of NH_4^+ and get some insights into the interactions between NH_4^+, SO_4^{2-}, and H_2O, a fitting process was applied to the spectra in this region as described in the experimental section. The operation is based on six peaks of NH_4^+ and H_2O according to previous literature,[35,36] which are shown in Table 1. The three peaks at 2878.7, 3032.1, and 3115.0 cm^{-1} are from NH_4^+, that is, the second overtone of NH_4^+ umbrella bending, the combination band of NH_4^+ umbrella bending with rocking vibrations, and the NH_4^+ symmetric stretching vibration.[35,36] The other three peaks at 3248.9, 3468.4, and 3628.8 cm^{-1} are assigned to the strongly, weakly, and slightly (more weakly) hydrogen-bonded components of water. The Raman spectra as dotted lines at various RHs in the 2400−4000 cm^{-1} region and the corresponding fitted bands as solid lines are shown in Figure 5, in which the six component peaks as dashed lines and the coefficient of determination (R^2) are also given. In our fitting, the frequency and the fwhm of each peak are kept constant at all RHs, as well as the relative area of the three NH_4^+ bands.

The areas of the six fitted components at various RHs are calculated and displayed in Figure 6, in which parts a and b correspond to the fitted components of NH_4^+ and water molecules, respectively. It is obvious that the areas of the three

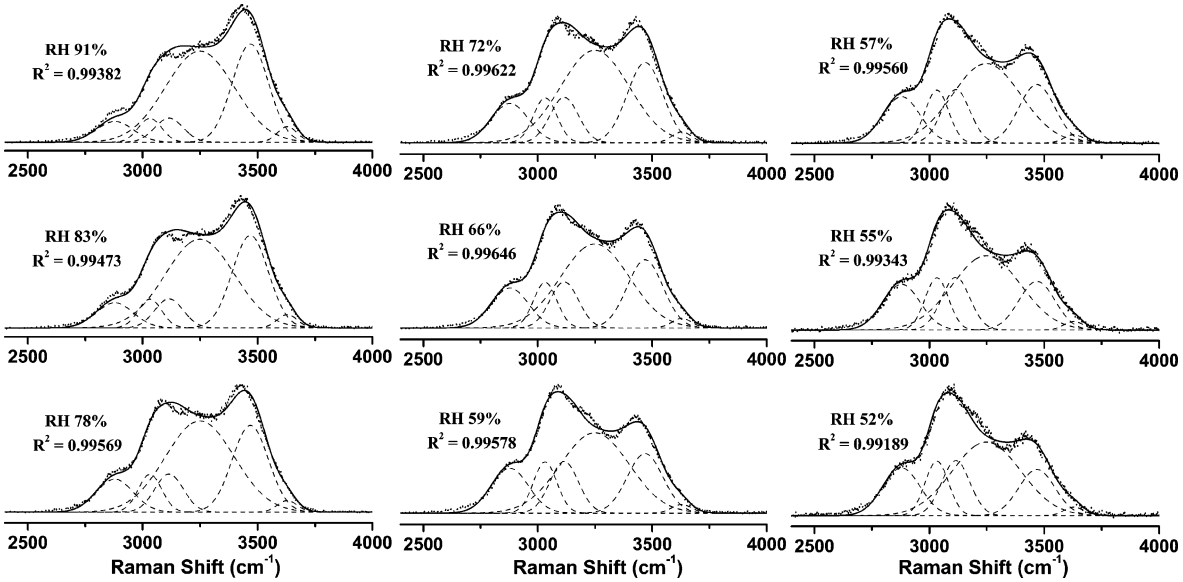

Figure 5. Experimental and fitted spectra in the region of 2400−4000 cm^{-1}. Dotted lines: the experimental Raman spectra. Dashed lines: the six fitted spectral components. Solid lines: the sum spectra of the six fitted spectral components. R^2: the coefficient of determination.

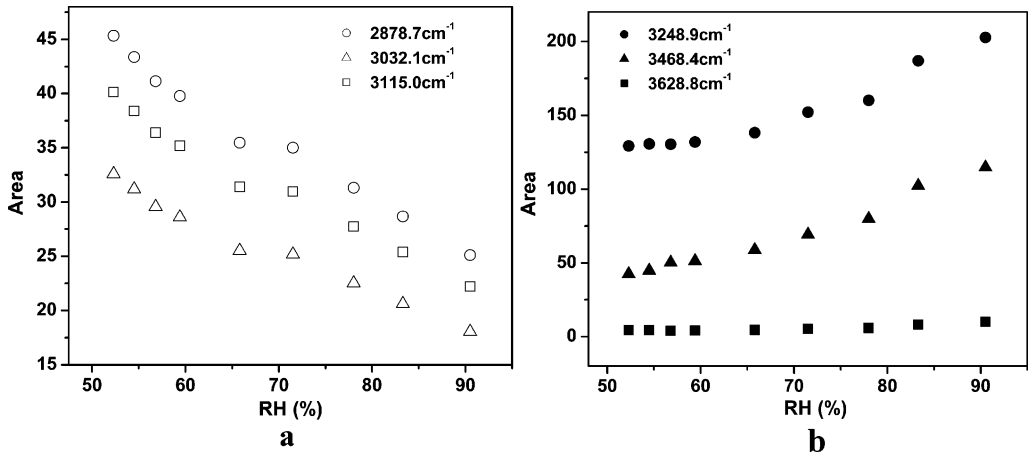

Figure 6. The areas of the six fitted components at various RHs. (a) The three peaks of NH_4^+ at 2878.7, 3032.1, and 3115.0 cm^{-1}; (b) the three peaks of H_2O at 3248.9, 3468.4, and 3628.8 cm^{-1}.

peaks related to NH_4^+ increase as the RH decreases as shown in Figure 6a. As expected, all three band components of the water O−H stretching envelope in Figure 6b weaken on the whole, in spite of the different decreasing rates of the band intensity with decreasing RH. According to spectral fittings, contributions from NH_4^+ can be removed to extract the H_2O bands from the complex envelope. Thus, the hygroscopic properties of $(NH_4)_2SO_4$ droplets can be evaluated by the ratio of the total areas of the three H_2O bands to the area of the υ_1-SO_4^{2-} band as a function of RH in the dehumidifying process as shown in Figure 2 (solid triangles), which is in accordance with WSR-RH curve.

Since the fitted spectra have already been normalized to the intensity of the υ_1-SO_4^{2-} band, it is predicted that the intensities of the bands ascribed to NH_4^+ should be invariable. However, as shown in Figure 6a, all intensities increase with a decrease of the RH. This discrepancy indicates that the Raman scattering cross sections of NH_4^+ vibrational modes all increase with respect to that of the υ_1-SO_4^{2-} band with the decrease of RH.

Interaction Similarities between NH_4^+, SO_4^{2-}, and H_2O. It has long been known that in solutions, NH_4^+ conspicuously resembles H_2O in several respects, including molar masses, bond angles, interatomic distances, and partial molar volumes. Particularly, the hydrogen bonds formed by H_2O and by NH_4^+ are similar in strength.[32] According to the relative partial molar entropy of water in aqueous electrolyte solutions, Frank and Robinson concluded that NH_4^+ is conducive to the stabilization of water structures by virtue of its tetrahedral shape and its ability to form hydrogen bonds.[37] On the other hand, Fajans and Johnson found that the apparent molar volume of NH_4Cl is approximately equal to that of two moles of water.[33] They further discussed that NH_4Cl near 35 °C resembles water most, and NH_4Cl is one of the salts producing the smallest changes in other properties of water such as entropy, viscosity, infrared absorption, and electron diffraction. It was explained as resulting from the fact that NH_4^+ fits into the tetrahedral structure of liquid water due to its four protons.[33] Kaminsky also reached the same conclusion that NH_4^+ hardly exerts any influence on the viscosity and structure of water.[38] In a study of nuclear magnetic resonance effects in aqueous solutions of 1−1 electrolytes, Hindman pointed out that dissolution of NH_4Cl does not markedly affect the proton resonance of water and ascribed the small experimental shift to chloride ion.[39]

The experimental number of water molecules in the first hydration layer of NH_4^+ has not been unambiguously determined.[40] Using the OPLS (optimized potentials for liquid simulations) set of intermolecular potential functions, Jorgensen and Gao figured out that NH_4^+ had about five strongly bound

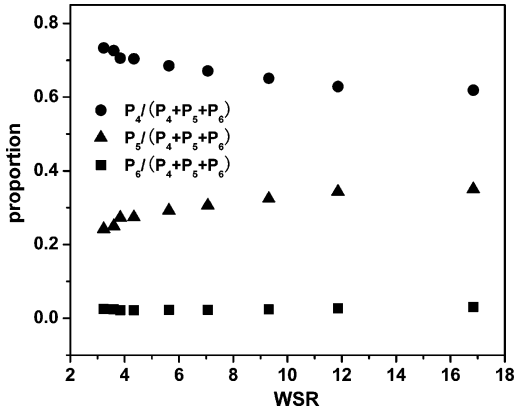

Figure 7. The proportions of three fitted water components in the $(NH_4)_2SO_4$ droplets at various WSRs. (Circles, triangles, and squares indicate strongly, weakly, and slightly hydrogen-bonded components, respectively.)

water molecules in the first hydration layer.[41] Furthermore, there was other evidence supporting the strong and directional hydrogen bonds between NH_4^+ and H_2O. In the gas phase, the experimental hydration enthalpy of the addition of a water molecule to the cluster ion $(NH_4^+)\cdot nH_2O$ ($n = 0-4$) is 10.6−20.6 kcal/mol.[42] Moreover, NH_4^+ is known to match well the lattice of water, and NH_4Br in 18-crown-6 displays the protons in directional hydrogen bonds between the NH_4^+ ions and the O atoms of 18-crown-6.[43] In addition, according to the intermolecular interactions, a cation−neutral complex of $NH_4^+\cdot\cdot\cdot H_2O$ has been assigned to a strong complex.[44]

SO_4^{2-} is considered to be a "structure maker" and can form hydrogen bonds with water molecules surrounding its tetrahedral structure.[30,45] Despite the fact the hydrogen bonds between SO_4^{2-} and water molecules are actually slightly stronger than those between water molecules,[46] Walrafen found that SO_4^{2-} produced only small effects on the water structure through Raman investigations.[47,48] Because the intensity of Raman scattering should increase with the decrease of bond polarity, Walrafen further attributed the small effects to the fact that those $HOH\cdots OSO_3^{2-}$ bonds were not greatly different from the $HOH\cdot\cdot\cdot OH_2$ bonds.[47] Similar spectroscopic features were also observed from the Fourier transform infrared-attenuated total reflectance (FTIR-ATR) spectra for sulfate solutions.[46]

It is reasonable that the areas of all three components of water decrease with WSR because of the evaporation of water, as indicated by the fitted spectra in Figure 6b. In order to further analyze the changes of three water components with WSR, their relative contents were evaluated according to the area ratios of their respective peaks to the whole water O−H stretching envelope, as shown in Figure 7. It is obvious that the proportion of the strongly hydrogen-bonded components increases, while that of the weakly hydrogen-bonded components decreases with WSR decreasing. It is well-known that the hydrogen bonds in the five-molecule tetrahedral structure are strong, while those in other structures are weak.[49] Therefore, at WSR = 16.8, strongly hydrogen-bonded components should mainly come from the five-molecule tetrahedral structure of water and the water molecules in the first shell of NH_4^+ and SO_4^{2-} ions. With the evaporation of water, the probability of collision of H_2O with NH_4^+ and SO_4^{2-} increases, while that between water molecules decreases, resulting in an increasing proportion of strongly hydrogen-bonded components and a decreasing proportion of weakly hydrogen-bonded ones. With a further decrease of the WSR, water molecules are likely to be fitted into the framework formed by NH_4^+ and SO_4^{2-} through the formation of hydrogen bonds, that is, the H and O atoms in water molecules interact with the O atoms of SO_4^{2-} and the H atoms of NH_4^+, respectively. The hydrogen bonds formed in such structures should be strong, which accounts for the further increase of the proportion of strongly hydrogen-bonded components. According to the two-species model proposed by Scherer et al., those water molecules forming strong hydrogen bonds on both hydrogen atoms, denoted as "···HOH···" should center at lower frequency, while those forming one strong hydrogen bond, denoted as "···HOH·····", should occur at higher frequency.[50]

It is obvious that the component at 3628.8 cm^{-1} can be resolved in the whole RH region. This component has been observed in Raman spectra of liquid water and HDO in D_2O, and was considered to be one of the spectral features of nonhydrogen-bonded O−H interactions.[51,52] However, instead of the muliticomponents model, strong new evidence disclosed in recent years may have finally tipped the balance in favor of the continuum model, according to which the hydrogen-bonding network weakens in a monomodal manner when going to higher frequencies.[53] This peak at 3628.8 cm^{-1} should better be attributed to the water molecules in the network whose angles and distances of hydrogen bonds significantly depart from the fully hydrogen-bonded five-molecule tetrahedral nearest-neighbor structure. In this work, the constant existence of this mode even in supersaturated $(NH_4)_2SO_4$ droplets indicates that there is a similar residence time for the water molecules fitted into the framework formed by NH_4^+ and SO_4^{2-} and those included in the hydrogen-bonding structures of pure water. In other words, there is a dynamic similarity for the water molecules in pure water and supersaturated $(NH_4)_2SO_4$ droplets.

Conclusions

By using micro-Raman spectroscopy, we have obtained the high S/N spectra of the $(NH_4)_2SO_4$ droplets in highly concentrated states without MDRs, which were frequently encountered in EDB measurements. With the decrease of RH, there is only a red-shift of 1.1 cm^{-1} in peak position and a slight broadening of 1.5 cm^{-1} in fwhm for the ν_1-SO_4^{2-} band in $(NH_4)_2SO_4$ droplets. Therefore, we concluded that the formation of the ion pairs between NH_4^+ and SO_4^{2-} has little effect on the spectral features of SO_4^{2-} and that $(NH_4)_2SO_4$ solutions are a qualified model of undisturbed sulfates even in supersaturated states. The O−H stretching region of water was fitted by six components to derive information on the interactions between ions and water molecules. From the results of fittings, we can describe the change of various water components in $(NH_4)_2SO_4$ droplets from dilute to supersaturated states. The proportion of the strongly hydrogen-bonded components was found to increase at the expense of weakly hydrogen-bonded ones with a decrease in the RH. The developing distributions with RH of water components with various hydrogen-bond features in $(NH_4)_2SO_4$ aerosol droplets may have some important implications on heterogeneous reactions occurring in the atmosphere.

Acknowledgment. This work was supported by the NSFC (20073004, 20473012, 20673010) and by the 111 Project B07012; the Trans-Century Training Program Foundation for the Talents by the Ministry of Education of China is also gratefully acknowledged.

References and Notes

(1) Posfai, M.; Anderson, J. R.; Buseck, P. R.; Shattuck, T. W.; Tindale, N. W. *Atmos. Environ.* **1994**, *28*, 1747.

(2) Chelf, J. H.; Martin, S. T. *J. Geophys. Res., Atmos.* **2001**, *106*, 1215.
(3) Prenni, A. J.; Wise, M. E.; Brooks, S. D.; Tolbert, M. A. *J. Geophys. Res., Atmos.* **2001**, *106*, 3037.
(4) Heintzenberg, J. *Tellus* **1989**, *41B*, 149.
(5) Penner, J. E.; Andreae, M.; Annegarn, H.; Barrie, L.; Feichter, J.; Hegg, D.; Jayaraman, A.; Leaitch, R.; Murphy, D.; Nganga, J.; Pitari, G. Aerosols, their direct and indirect effects. In *Climate Change 2001: The Scientific Basis*. *Contribution of Working Group I to the Third Assessment Report of the Intergovernmental Panel on Climate Change*; Houghton, J. T., Ding, Y., Griggs, D. J., Noguer, M., Linden, P. J., Dai, X., Maskell, K., Johnson, C. A., Eds.; Cambridge University Press: New York, 2001; p 289.
(6) Martin, S. T. *Geophys. Res. Lett.* **1998**, *25*, 1657.
(7) Liou, K. N. *Mon. Weather Rev.* **1986**, *114*, 1167.
(8) Kane, S. M.; Caloz, F.; Leu, M. T. *J. Phys. Chem. A* **2001**, *105*, 6465.
(9) Hu, J. H.; Abbatt, J. P. D. *J. Phys. Chem. A* **1997**, *101*, 871.
(10) Orr, C., Jr.; Hurd, F. K.; Corbett, W. J. *J. Colloid Sci.* **1958**, *13*, 472.
(11) Tang, I. N.; Munkelwitz, H. R. *J. Aerosol Sci.* **1977**, *8*, 321.
(12) Tang, I. N.; Fung, K. H.; Imre, D. G.; Munkelwitz, H. R. *Aerosol Sci. Technol.* **1995**, *23*, 443.
(13) Cziczo, D. J.; Nowak, J. B.; Hu, J. H.; Abbatt, J. P. D. *J. Geophys. Res.* **1997**, *102*, 18843.
(14) Tang, I. N.; Munkelwitz, H. R. *J. Geophys. Res.* **1994**, *99*, 18801.
(15) Richardson, C. B.; Spann, J. F. *J. Aerosol Sci.* **1984**, *15*, 563.
(16) Cohen, M. D.; Flagan, R. C.; Seinfeld, J. H. *J. Phys. Chem.* **1987**, *91*, 4563.
(17) Rood, M. J.; Shaw, M. A.; Larson, T. V.; Covert, D. S. *Nature* **1989**, *337*, 537.
(18) Chan, C. K.; Flagan, R. C.; Seinfeld, J. H. *Atmos. Environ.* **1992**, *26A*, 1661.
(19) Parsons, M. T.; Knopf, D. A.; Bertram, A. K. *J. Phys. Chem. A* **2004**, *108*, 11600.
(20) Martin, S. T.; Han, J. H.; Hung, H. M. *Geophys. Res. Lett.* **2001**, *28*, 2601.
(21) Rudolph, W. W.; Mason, R. *J. Solution Chem.* **2001**, *30*, 527.
(22) Rudolph, W.; Irmer, G. *J. Solution Chem.* **1994**, *23*, 663.
(23) Rudolph, W.; Brooker, M. H.; Tremaine, P. R. *J. Solution Chem.* **1997**, *26*, 757.
(24) Zhang, Y. H.; Chan, C. K. *J. Phys. Chem. A* **2002**, *106*, 285.
(25) Wang, F.; Zhang, Y. H.; Li, S. H.; Wang, L. Y.; Zhao, L. J. *Anal. Chem.* **2005**, *77*, 7148.
(26) Xu, J.; Imre, D.; McGraw, R.; Tang, I. *J. Phys. Chem. B* **1998**, *102*, 7462.
(27) Chatterjee, R. M.; Adams, W. A.; Davis, A. R. *J. Phys. Chem.* **1974**, *78*, 246.
(28) Rull, F.; Balarew, C.; Alvarez, J. L.; Sobron, F.; Rodriguez, A. *J. Raman Spectrosc.* **1994**, *25*, 933.
(29) Pye, C. C.; Rudolph, W. W. *J. Phys. Chem. A* **1998**, *102*, 9933.
(30) Pye, C. C.; Rudolph, W. W. *J. Phys. Chem. A* **2001**, *105*, 905.
(31) Watanabe, D.; Hamaguchi, H. *J. Chem. Phys.* **2005**, *123*, 034508.
(32) Vollmar, P. M. *J. Chem. Phys.* **1963**, *39*, 2236.
(33) Fajans, K.; Johnson, O. *J. Am. Chem. Soc.* **1942**, *64*, 668.
(34) Jordanov, N.; Zellner, R. *Phys. Chem. Chem. Phys.* **2006**, *8*, 2759.
(35) Spinner, E. *Spectrochim. Acta, Part A* **2003**, *59*, 1441.
(36) Gopalakrishnan, S.; Jungwirth, P.; Tobias, D. J.; Allen, H. C. *J. Phys. Chem. B* **2005**, *109*, 8861.
(37) Frank, H. S.; Robinson, A. L. *J. Chem. Phys.* **1940**, *8*, 933.
(38) Kaminsky, M. *Discuss. Faraday Soc.* **1957**, *24*, 171.
(39) Hindman, J. C. *J. Chem. Phys.* **1962**, *36*, 1000.
(40) Kassab, E.; Evleth, E. M.; Hamou-Tahra, Z. D. *J. Am. Chem. Soc.* **1990**, *112*, 103.
(41) Jorgensen, W. L.; Gao, J. *J. Phys. Chem.* **1986**, *90*, 2174.
(42) Meot-Ner, M. *J. Am. Chem. Soc.* **1984**, *106*, 1265.
(43) Nagano, O.; Kobayashi, A.; Sasaki, Y. *Bull. Chem. Soc. Jpn.* **1978**, *51*, 790.
(44) Kollman, P. *J. Am. Chem. Soc.* **1977**, *99*, 4875.
(45) Cannon, W. R.; Pettitt, B. M.; McCammon, J. A. *J. Phys. Chem.* **1994**, *98*, 6225.
(46) Wei, Z. F.; Zhang, Y. H.; Zhao, L. J.; Liu, J. H.; Li, X. H. *J. Phys. Chem. A* **2005**, *109*, 1337.
(47) Walrafen, G. E. *J. Chem. Phys.* **1962**, *36*, 1035.
(48) Walrafen, G. E. *J. Chem. Phys.* **1971**, *55*, 768.
(49) Liu, J. H.; Zhang, Y. H.; Wang, L. Y.; Wei, Z. F. *Spectrochim. Acta, Part A* **2005**, *61*, 893.
(50) Scherer, J. R.; Go, M. K.; Kint, S. *J. Phys. Chem.* **1974**, *78*, 1304.
(51) Walrafen, G. E. *J. Chem. Phys.* **1969**, *50*, 560.
(52) Carey, D. M.; Korenowski, G. M. *J. Chem. Phys.* **1998**, *108*, 2669.
(53) Smith, J. D.; Cappa, C. D.; Wilson, K. R.; Cohen, R. C.; Geissler, P. L.; Saykally, R. J. *Proc. Natl. Acad. Soc. U.S.A.* **2005**, *102*, 14171.